Peer-reviewed version available at Magnetochemistry 2018, 4, 35; doi:10.3390/magnetochemistry4030035

Article

Magneto-Optic Surface Plasmon Resonance Ti/Au/Co/Au/Pc Configuration and Sensitivity

Conrad Rizal[1]

[1] Electrical Engineering & Computer Science, York University, Toronto, ON, M3J 1P3 Canada
[2] GEM Systems Inc, Markham, ON, L3R 5H6 Canada (Conrad.Rizal@gemsys.ca)
*Correspondence: crizal@yorku.ca; Tel.: +1-647-570-4039

Abstract:

Magneto-optic surface plasmon resonance (MOSPR) based sensors are highly attractive as next generation biosensors. However, these sensors suffer from oxidation leading to degradation of performance, reproducibility of the sensor surface because of the difficulty of removing adsorbed materials, and degradation of sensor surface during surface cleaning, and these limit their applications. In this paper, I propose MOSPR-based biosensors with 0 to 15 nm thick inert polycarbonate laminate plastic as a protective layer and theoretically demonstrate the practicability of our approach in water-medium for three different probing samples: ethanol, propanol, and pentanol. I also investigate microstructure and magnetic properties. The chemical composition and layered information of the sensor are investigated using X-ray reflectivity and X-ray diffraction analyses and these show distinct fcc-Au (111) phases, as dominated by the higher density of conduction electrons in Au as compared to Co. The magnetic characterization measured with the in-plane magnetic field to the sensor surface for both the as-deposited and annealed multilayers showed isotropic easy axis magnetization parallel to the multilayer interface at a saturating magnetic field of < 100 Oe. The sensor showed a maximum sensitivity of 5.5×10^4% / RIU for water-ethanol media and the highest detection level of 2.5×10^{-8} for water-pentanol media as the protective layer is increased from 0 to 15 nm.

Keywords: Ti/Au/Co/Au, X-ray diffraction, MOSPR, sensitivity, polycarbonate plastics

1. Introduction

Artificially-tailored magneto-optic (MO) Ta/Au/Co/Au structures are interesting materials for investigating magnetic (magnetization, magnetic anisotropy, etc.), microstructure (crystal structure, multilayer interface and surface roughness, etc.), surface plasmon resonance (SPR) and magneto-optics SPR effects arising from magneto-plasmonics (MPs) – the interaction of magnetic field with surface plasmon polariton and correspondingly induced MO properties, and these have huge potentials for applications, for details, see [1-3]. New functionality can be achieved from the combined roles of generating surface plasmon oscillations in the artificially tailored MP structures, when excited by an TM polarized (p-polarized) optical radiation that are further controlled by external magnetic fields [4]. The excitation condition strongly depends on the magnetic properties such as magnetic permeability, susceptibility, direction of magnetic spin orientation, microstructure properties such as metal-dielectric and metal-metal interface states, dielectric properties such as permittivity or the permeabilities of the layers involved, and MO properties such as MO coefficients (permittivity or permeability changes due to the interaction magnetic, H fields with optical radiation and surface plasmon polaritons) [5].

Ti/Au/Co/Au/P_c is one of the most important artificially-tailored MO nanostructured multilayers that has recently seen huge potential in the field of bio-sensing and imaging [6-9] (t_{pc} denotes the thickness of protective layer here). The choice of Au in this configuration is due to its excellent plasmonic properties arising from the high electron density of about 25×10^{22} cm^3 (Au possess an abundance of surface plasmons), its low electrical resistivity, and least chemical reactivity. All these features are essential in reducing attenuation and enhancing plasmon activity. Likewise, the choice of Co as a MO material is due to its excellent H field-dependent property, as pure Co is ferromagnetic with the magnetic moment, μ_B/atom of 0.7 (saturation magnetization, M_s of 172 emu/gm at room temperature), density of 8.9 gm/cm^3, Curie temperature, T_C, of 1115 ^{0}C, and complex relative permittivity, ε_r of -16.493 + j23.337 at λ = 785 nm (μ_B is the magnetic unit expressed in Bohr unit). Due to the high magnetic moment, it offers the possibility of having strong magnetic modulation of permittivity at room temperature when excited by an optical radiation near infra-red. By combining plasmonic Au and ferromagnetic Co properties into Ti buffer and polycarbonate t_{pc} layer, and by optimizing the configuration, the influence of SPs and magnetism on sensitivity and device performance can be exploited [9-17].

As reported by us earlier [18] and the references cited therein as well as by many others [7, 19], several modulation approaches have been explored to enhance the sensitivity of the SPR-based sensors. Depending on the motivation of measurement, two approaches have been employed to investigate the sensitivity of MOKE-based sensors: One is differential reflectivity change, $\Delta R(n)$ due to modulating H field, and another is normalized reflectivity, again due to modulating magnetic field expressed as, [RpH(+)-RpH(-)]/[RpH(+)+RpH(-)], where RpH(+) and RpH(-) are reflectivity in the presence of applied magnetic field in the positive and negative directions, respectively [9, 17]. In the present case, the sensitivity is calculated using:

$$\text{Sensitivity} = \frac{\mathrm{d}\left[\frac{R_p\mathrm{H}(\pm) - \mathrm{RpH}(0)}{R_{pH}(0)}\right]}{dn} \times 100\ [\% / \mathrm{RIU}] \quad (1)$$

where $\Delta Rp = RpH(\pm) - RpH(0)$ is the differential reflectivity change due to modulating magnetic field and it is normalized by $R_{pH}(0)$. The normalized differential reflectivity change was calculated for all three probing samples (ethanol, pentanol, and propanol) with reference to the differential reflectivity change in the water-medium. The differential reflectivity change is normalized again with the differential refractive index change (Δn) between the probing sample and water-medium. RpH($\pm$) and RpH(0) are the reflectivities in the presence and absence of applied H fields, respectively.

Despite the higher sensitivity and improved performances shown by the MO-based SPR sensors, several technical challenges still prevail such as, oxidation of sensor surface leading to degradation of performance, issues with reproducibility of the sensor surface due to the difficulty of removing adsorbed materials and scratching of sensor surface during cleaning. In addition to the composition and layer thickness, interface roughness between each layer of the sensor configuration also plays critical roles in defining MO effect and sensitivity of the sensor [7].

To better understand the light-matter interaction, and magnetic and microstructure properties, in this paper, I explore magneto-optic (MO) Ti/Au/Co/Au/Pc multilayers using Quantum design vibrating sample magneto-meter / p-MOKE magnetometer and X-ray diffractometers, respectively. I analyze the MO effect using transfer matrix method similarly to what has been described in our prior work [20]. Both variations in optical excitation wavelength and probed medium are also taken into consideration in the analysis. Furthermore, I have studied the effect of protective layer, t_{Pc} (nano-sized polycarbonate plastic of permittivity of 2.50) on the sensitivity and have proposed and demonstrated the practicability of the approach. Three types of alcohol samples, namely, ethanol, pentanol and propanol, with increasing molecular weight and refractive index are used as probing

Peer-reviewed version available at Magnetochemistry 2018, 4, 35; doi:10.3390/magnetochemistry4030035

87 samples. The study shows that the protective layer does not compromise the MO enhancement and
88 sensitivity. The proposed sensor configuration is an excellent candidate for developing robust
89 practical bio-sensor.

90 **2. Microstructure Study**

91 High angle X-ray diffraction (XRD) or low angle X-ray reflection (XRR) analyses are widely used to
92 characterize many unknown nano-structured materials in the field of geology, environmental
93 science, material science, engineering, and biology, to name a few [21]. While XRD is primarily used
94 to determine crystal structure, lattice mismatch between the substrate and individual layers due to
95 stress or strain, dislocation density and quality of the nano-structure multilayer films, XRR is used
96 to determine the layer or bilayer thickness, surface or interface roughness and density of the film.
97 These studies help us to understand better light-matter interaction and relationship between
98 crystallographic plane and magneto-optics properties that are essential for bio-sensing.

99 Figure 1 shows the high-angle out-of-plane X-ray diffraction (XRD) profiles measured for both the
100 as-deposited (shown by blue curve) and annealed (shown by red curve) dc-sputtered Ti/Au/Co/Au
101 configuration corresponding to the (111) textured growth. The profile shows a peak at average inter-
102 planar distance of Co and Au. The high intensity diffraction peaks indicate the presence of Au (111),
103 Au (222) and Co (111) planes parallel to the surface. As shown in it, the position of peaks slightly
104 shifted towards higher angles after annealing, similarly to our nano-scale Co/Au multilayer
105 reported earlier [22]. However thicker layers showed signature of Au (222) and Co (111) and Co
106 (002) planes in addition to the (111) planes. In all the cases, reflection peaks are characteristically
107 sharp and they can be explained using [21] as:

$$2 \sin \theta_x = \frac{1}{\hat{d}} + \frac{n}{\Lambda} \quad (2)$$

108 where, n is the order of the satellite peaks around the main Bragg peak, and θ_x is Bragg's angle. The
109 sharpness of the peak indicates good interface coherence and highly crystalline morphology along
110 the surface normal to the substrate.

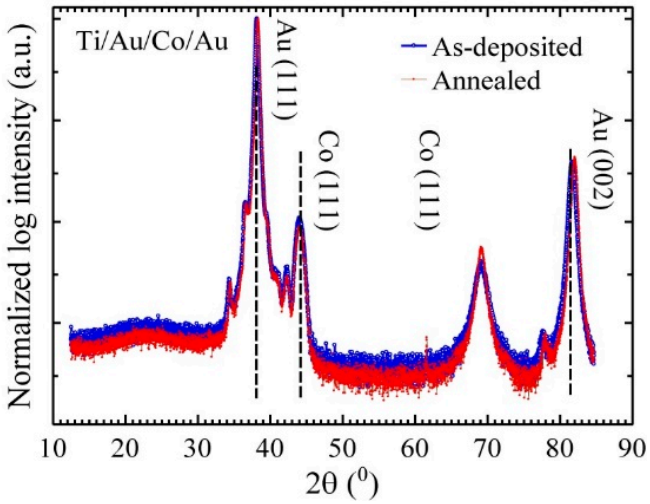

111

112 **Fig. 1** Comparison of XRD profiles for the as-deposited and annealed Ti/Au/Co/Au samples.

113 Figure 2 shows the results of a low angle reflectivity (XRR) profiles of Ti/Au/Co/Au structure as
114 analyzed using X-ray diffractometer. The profile shows several peaks at average interplanar distance
115 of Co and Au and is controlled by the refractive index of Ti, Au and Co layer. The refractive index is

related to the atomic density and scattering power of individual elements, in this case, again, Ti, Au and Co.

The XRR profile of the multilayer is dominated by the total thickness since the real parts of the indices of refraction in this case are almost equal ($n_{Au} \approx 0.99$, $n_{Co} \approx 0.85$, and $n_{Ti} \approx 0.998 < 1.0$ at the X-ray wavelength, λ of 0.000154 μm [23]). Moreover, the profile is not only depending on the total thickness but also on all four layers and interface between each of them. This possess problems in separating discrete (ρ_d) from continuous roughness (ρ_c) one [24]. Note that the roughness caused by atomic level roughness is termed as a continuous roughness and can vary continuously through-out the multilayer. It arises from lattice mismatch at the interface between two layers, dislocation, layer thickness variation, etc. Whereas, discrete roughness is associated with layer thickness consisting of integer number of atomic layers and it usually results from non-uniform growth modes. The detailed discussion of these roughness is beyond the scope of this paper. Interested readers are referred to [24, 25].

Overall roughness is given by $\rho = \sqrt{(\rho_c^2 + \rho_d^2)}$ where, ρ_c and ρ_d are continuous and discrete disorder, respectively, and can also arise from the Ti buffer and substrate roughness

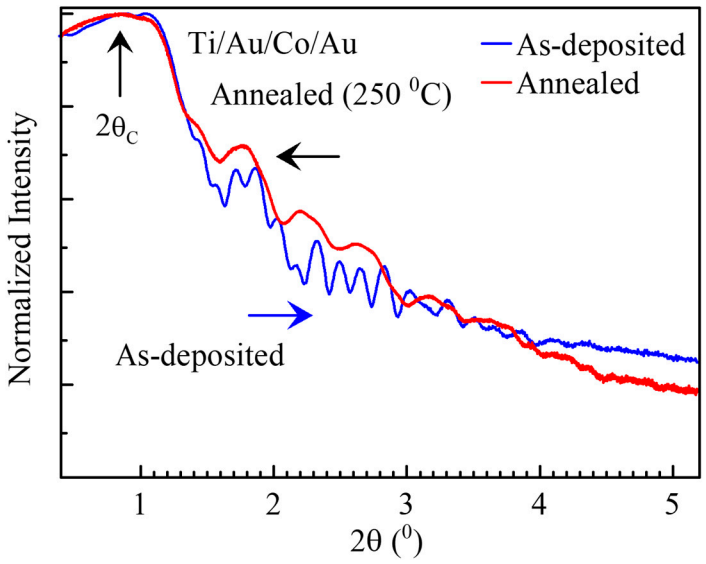

Fig. 2 Comparison of XRR profiles of as-deposited (denoted by blue) and annealed (denoted by red). The blue horizontal arrow shows the direction of increasing roughness.

The beating seen in the measured XRR profiles in Figure 2 can arise either from the oxidation of the buffer layer or surface roughness of both buffer layer and substrate. Discrete roughness can also be a cause of the beating. After annealing, the dip in the reflection peaks is further reduced suggesting the improvement of the surface of the buffer layer. For additional information about roughness, I refer interested readers to our prior work [20].

3. Magnetic Characterization

The effect of interaction of the magnetic field, H with optical radiation for paramagnetic or diamagnetic matter is very small at normal intensities and can be neglected. However, in the present work, in ferromagnetic multilayers consisting of Co, the interaction of light with the magnetic moment of Co has two effects depending on whether the incident optical radiation is TM-polarized (p-polarized) or TE-polarized (s-polarized) with respect to the orientation of magnetic moment. For the TM-polarized light, a direct relationship exists between the interaction of optical radiation and

magnetism (M_s - saturation magnetization) and correspondingly induced dielectric tensor of Co, known as magneto-optic (MO) coefficient. The MO effect is directly related to the orientation of magnetic moment or the direction of applied field in the sensor configuration and therefore, magnetic measurement is important to understand the physics of light-matter interaction in multilayer configuration.

If a TM-polarized (p-polarized) light is perpendicularly incident on the sensor surface, the light is purely reflected (this is further discussed in section 5) meaning that the orientation of magnetic moment in Co has strong effect on whether the light gets reflected or rotated. Figure 3 shows the normalized M-H curves of the as-deposited and annealed samples, measured with the in-plane magnetic field, H swept between ± 10 kOe. The inset in the right shows enlarged view of the M-H curves, with a coercive force, H_c of 40 Oe. Both the in-plane and perpendicular-to-plane of the tri-multilayer surface (only in-plane measured M-H curves are shown here) for both the as-deposited and annealed samples showed isotropic in-plane easy axis magnetization along the multilayer interface. The saturation magnetization, M_s, for the as-deposited structure is found to be 1407 emu/cm^3 and it decreased to 1233 emu/cm^3 after annealing at 250^{0}C for 30 minutes. Unlike our nano-scale Co (1 nm) /Au (2 nm) multilayers reported earlier [21], the M_s in multilayer with 8 nm thick Co layer slightly decreases after annealing. It seems that the interface states between the Au and Co is primarily responsible for this decrease. This information will be very useful to develop a practical biosensor.

As shown by the M-H curves, the multilayer configuration shows easy axis along the multilayer surface (for the configuration, see, Figure 5) That is, the orientation of magnetic moments in the 8 nm thick Co layer are along the interface between Co and Au. This configuration is further discussed in section 5. The magnitude of coercive force suggests that only a small amount of H field is needed to saturate or rotate the magnetic spin in the transverse direction, i.e., parallel to the interface.

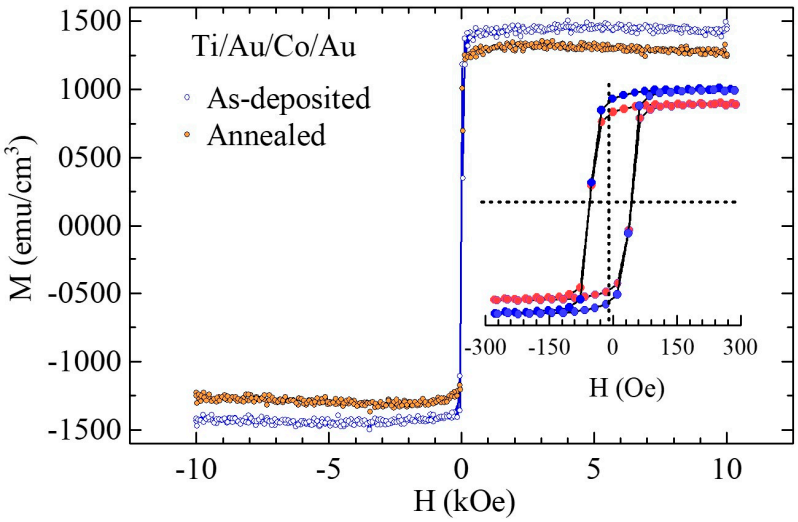

Fig 3 M-H characteristics of the as-deposited and annealed samples plotted against the H field. Inset shows the enlarged view measured at ± 300 Oe.

4. MO-SPR Sensitivity and Protective Layer

Figure 4 shows normalised MOSPR sensitivity curves plotted against incident angles with increasing protective layer thickness, $t_{Pc} = 0$ to 15 nm, calculated in water-medium for 3 different probing bio-samples, namely, ethanol, propanol, and pentanol. The protective layer is an inert and transparent plastic (polycarbonate, in this case) with permittivity of 2.51 at $\lambda = 785$ nm.

Preprints (www.preprints.org) | NOT PEER-REVIEWED | Posted: 30 July 2018 doi:10.20944/preprints201807.0587.v1

Peer-reviewed version available at Magnetochemistry 2018, 4, 35; doi:10.3390/magnetochemistry4030035

Figure 4 (a) shows normalized sensitivity of the sensor without a protective layer i.e., t_{Pc} = 0 nm. The maximum MOSPR sensitivity occurs at the excitation angle, θ of 41.51° for water-ethanol media and the peak slightly shifts towards higher angle with increasing refractive indices, i.e., for water-propanol and water-pentanol media.

Figure 4 (b-d) show normalized sensitivity as the t_{pc} is increased from 5 to 15 nm (in the increment of 5 nm). The incident angle at which the maximum sensitivity occurs shifts towards higher angle with both increasing t_{pc} and increasing differential refractive index, dn. In this scheme, the magnitude of this signal is dependent strongly on dn whereas the shift of maximal peak position is dependent on t_{pc} (the t_{pc} did not have any adverse effect towards the sensitivity). In all cases, the MOSPR peaks are sharper and show higher gradients compared to the conventional SPR sensors meaning increased signal-to-noise ratio when operated either at angular and/or intensity interrogation modes [14]. All the calculated parameters are listed in Table 1.

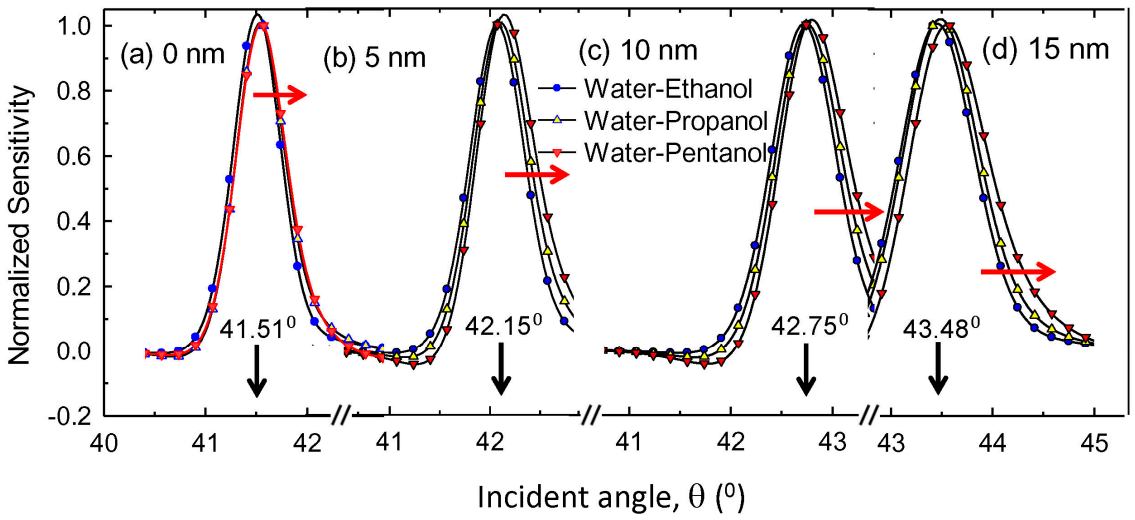

Fig. 4 Plot of normalized sensitivity recorded for three different alcohol samples with an increasing refractive index in water medium with respect to water medium. (a) Sensor without protective layer and (b-d) sensor with protective layer, increased from 5 to 15 nm. The vertical black arrows indicate the position of reflectivity minima observed for pure water medium. The red horizontal arrows indicate direction of peak shift with differential refractive index change.

Table 1: Optical parameters for water-based media. In column 2, the quantity inside the bracket denotes the thickness of the protective layer, t_{Pc}. The detection noise, $\sigma = 5.0\times10^{-4}$ was obtained from literature [26], S and D denote sensitivity and detection level, respectively.

Probing media (Δn at λ 785 nm)	Incident angle, θ°. The numbers within the bracket indicate the thickness of the protective layer (t_{pc}, in nm.				Sensitivity, S_{MOSPR} [% / RIU]	Detection level, D = σ/S (RIU)
water-ethanol (0.0281)	41.51° (0)	42.15° (5)	42.75° (10)	43.48° (15)	5.5×10^{4}	0.90×10^{-8}
water-propanol (0.0492)	41.60° (0)	42.20° (5)	42.85° (10)	43.60° (15)	3.2×10^{4}	1.56×10^{-8}
water-pentanol (0.0732)	41.70° (0)	42.30° (5)	42.95° (10)	43.72° (15)	2.0×10^{4}	2.50×10^{-8}

Peer-reviewed version available at Magnetochemistry 2018, 4, 35; doi:10.3390/magnetochemistry4030035

Table 1 lists the MOSPR sensitivity obtained from Figure 4. For simplicity, only the normalised curves are shown here. As shown in it, the maximum MO-SPR sensitivity in water medium is found to be around 5.5×10^{4} % / RIU (refractive index unit) and the highest is for water-ethanol (i.e., smaller change in refractive index, dn). This value is almost one order larger compared to the sensitivity of the SPR-based sensor (≈ 10^{3} % / RIU (SPR sensitivity is not shown here for simplicity). The detection level increased with increasing differential refractive index change of the tested samples, and the highest is for water-pentanol media (2.5×10^{-8} RIU). For the study of variation of Co and Au layer thicknesses on the MOSPR sensitivity, I refer interested readers to our prior work [18].

5. Materials and Methods

A typical proposed MOSPR sensor configuration is shown in Figure 5. It consists of Au(t_{Au}) / Co(t_{Co}) / Au(t_{Au}) multilayers including Ti buffer layer. The samples were prepared by depositing Ti buffer layer first on glass substrate and then depositing Au and Co layers using dc-sputtering at vacuum pressure of 10^{-6} Torr., and at room temperature, where t_{Ti}, t_{Co}, and t_{Au} denote the thicknesses of Ti, Co, and Au layers, respectively.

The deposition method is as follows: First, a thin buffer layer of 2 nm of Ti (0.03 nm/s) was deposited on to the glass substrate surface. The buffer layer was not annealed. As the next step, a 35 nm of Au layer (0.07 nm/s) was deposited on the Ti buffer layers. After that, an 8 nm of Co (0.03 nm/s) was deposited on top of the Au layer. Finally, a 10 nm of Au layer was deposited on top of the Co layer. For further details on fabrication method, interested readers are referred to our recent paper [20]. Various geometrical and optical parameters are given in Table 2.

The M-H curves were measured using a Quantum Design vibrating sample magnetometer and p-MOKE magneto-meter with H swept at H = ±10 kOe for both the as-deposited and annealed samples. The microstructure was investigated using X-ray diffractometer at both low and high angles. I also performed theoretical fitting of the experimental data using *GenX* [27] but these are not shown here for simplicity. For further details on data fitting on similar structures, I refer interested readers again, to our prior work [21].

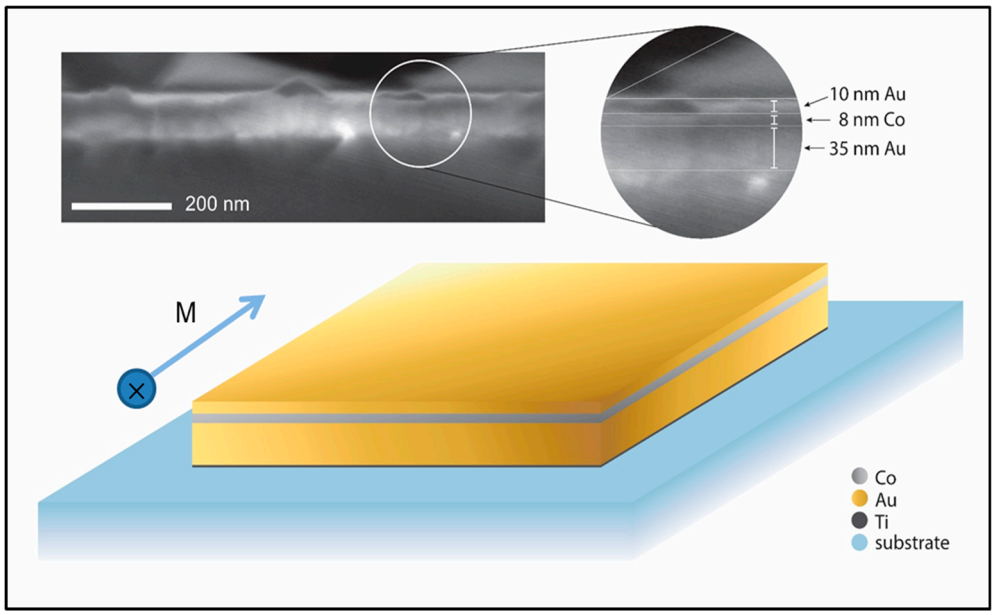

Fig. 5 Schematic of a fabricated sensor configuration (bottom). On the top left shown is the side view of the fabricated sensor studied using SEM. Enlarged view is shown in the top right. The orientation of magnetic spin is shown by large arrow that is parallel to the Co and Au interface.

Table 2: Optical parameters at λ = 785 used for modeling. ε_{moCo} is a magneto-optic constant, also known as off-diagonal tensor component (0.85+j0.0006) [5].

Materials	Symbol	Refractive index, n	Extinction Coeff., k	Real part ε_1	Imaginary Part, ε_2	Literature Source
Glass	BK-7	1.5111	9.22×10^{-9}	2.30	2.95×10^{-9}	[28]
Titanium	Ti	3.0937	4.01	-6.51	24.811	[29]
Gold	Au	0.14891	4.78	-22.86	1.4245	[29]
Cobalt	Co	2.4580	4.75	-16.49	23.337	[29]
Air	Air	1.000275	-	1.0055	-	[30]
Water	H_2O	1.3296	1.39×10^{-7}	1.7678	3.69×10^{-9}	[31]
Ethanol	C_2H_5OH	1.3577	-	1.8433	-	[32]
Propanol	C_3H_7OH	1.3788	-	1.9011	-	[33]
Pentanol	$C_5H_{11}OH$	1.4028	-	1.9678	-	[33])
Polycarbonate	$(C_{16}H_{14}O_3)_n$	1.5713	-	2.51	-	[34]

For the MO characterizations, the multilayer structure shown in Figure 5 were optically interfaced to a prism in Kretchmann configuration using an index matching fluid (i.e., matching liquid) between the glass substrate and prism surface, similarly to the configuration shown in [20]. The surface plasmon were excited using TM-polarized (p-polarized) optical radiation at a λ of 785 nm. In this work, the optical constants were obtained from literature (see, column 7 in Table 2) and the MO effects were modeled using transfer-matrix formalism. The literature MO coefficient for Co was obtained from [5]. The MO coefficients were set to zero and literature values under no external H field and under applied H field of a saturating magnetic field, respectively. The various dimensional and optical parameters used in the calculations and correspondingly used reference sources are listed in Table 2.

6. Conclusions

I experimentally investigated the micro-structural and magnetic properties of magneto-optical Ti/Au/Co/Au/Pc bio-sensor. Microstructure studies showed strong fcc-Au <111> phase for all the fabricated samples. Magnetic studies suggested isotropic behaviour with easy axis parallel to the Co/Au interface (transverse direction). The MO configuration showed a maximum sensitivity of 5.5×10^4 % / RIU (water-ethanol media). The highest detection level is found to be 2.5×10^{-8} RIU (water-pentanol media), which is comparable to or larger than the sensitivity of the recently reported SPR sensors [18]. This work opens the possibility of developing a practical bio-sensor with increased lifetime, improved performance and detection level of the sensor without compromising the sensor performance.

Acknowledgments: The author thanks James Wingert (member of the Shpyrko Group), Department of Physics, University of California, San Diego, for X-ray characterization, Mathew Rozin (member of the Tao Group), Department of Nanoengineering, University of California, San Diego, for SEM imaging, and Dr. Frederick E. Spada, Associate Research Scientist, Center for Memory and Recording Research (CMRR), University of California, San Diego for granting an access to the polar-MOKE device for magnetic characterization. The author acknowledges financial support received from NSERC and MITACS Inc., Canada and CMRR, UC San Diego, USA for this work.

Conflict of interest: The author declares no conflict of interest.

References

[1] C. Rizal, B. Niraula, and H. Lee, "Bio-magnetoplasmonics, emerging biomedical technologies and beyond," *Journal Nanomedicine Research,* vol. 3, no. 3, pp. 00059-00065, 2016.

[2] C. Rizal, B. Moa, and B. B. Niraula, "Ferromagnetic multilayers: Magnetoresistance, magnetic anisotropy, and beyond," *Magnetochemistry,* vol. 2, no. 2, p. 22, 2016.

[3] M. S. Kushwaha and P. Halevi, "Magnetoplasmons in thin films in the Voigt configuration," *Physical Review B,* vol. 36, no. 11, pp. 5960-5967, 10/15/ 1987.

[4] B. Diaz-Valencia, J. Mejía-Salazar, O. N. Oliveira Jr, N. Porras-Montenegro, and P. Albella, "Enhanced Transverse Magneto-Optical Kerr Effect in Magnetoplasmonic Crystals for the Design of Highly Sensitive Plasmonic (Bio) sensing Platforms," *ACS Omega,* vol. 2, no. 11, pp. 7682-7685, 2017.

[5] J. González-Díaz, B. Sepúlveda, A. García-Martín, and G. Armelles, "Cobalt dependence of the magneto-optical response in magnetoplasmonic nanodisks," *Applied Physics Letters,* vol. 97, no. 4, p. 043114, 2010.

[6] G. Armelles, A. Cebollada, A. Garcia-Martan, and M. U. Gonza¡lez, "Magnetoplasmonics: Combining magnetic and plasmonic functionalities," *Advanced Optical Materials,* vol. 1, no. 1, pp. 2-21, 2013.

[7] M. G. Manera, E. a. Ferreiro-Vila, J. M. Garcia-Martin, A. Garcia-Martin, and R. Rella, "Enhanced antibody recognition with a magneto-optic surface plasmon resonance (MO-SPR) sensor," *Biosensors and Bioelectronics,* vol. 58, pp. 114-120, 2014.

[8] E. T. Papaioannou *et al.*, "Magnetic, magneto-optic and magnetotransport properties of nanocrystalline Co/Au multilayers with ultrathin Au interlayers," *Journal of Nanoscience and Nanotechnology,* vol. 8, no. 9, pp. 4323-4327, 2008.

[9] D. Regatos, B. Sepúlveda, D. Fariña, L. G. Carrascosa, and L. M. Lechuga, "Suitable combination of noble/ferromagnetic metal multilayers for enhanced magneto-plasmonic biosensing," *Optics Express,* vol. 19, no. 9, pp. 8336-8346, 2011/04/25 2011.

[10] C. A. Herreño-Fierro, E. J. Patino, G. Armelles, and A. Cebollada, "Surface sensitivity of optical and magneto-optical and ellipsometric properties in magnetoplasmonic nanodisks," *Applied Physics Letters,* vol. 108, no. 2, p. 021109, 2016.

[11] T. Špringer, M. L. Ermini, B. Špačková, J. Jabloňků, and J. Homola, "Enhancing Sensitivity of Surface Plasmon Resonance Biosensors by Functionalized Gold Nanoparticles: Size Matters," *Analytical Chemistry,* vol. 86, no. 20, pp. 10350-10356, 2014/10/21 2014.

[12] T.-J. Wang, K.-H. Lee, and T.-T. Chen, "Sensitivity enhancement of magneto-optic surface plasmon resonance sensors with noble/ferromagnetic metal heterostructure," *Laser Physics,* vol. 24, no. 3, p. 036001, 2014.

[13] G. Pellegrini and G. Mattei, "High-performance magneto-optic surface plasmon resonance sensor design: an optimization approach," *Plasmonics,* vol. 9, no. 6, pp. 1457-1462, 2014.

[14] M. Piliarik and J. Homola, "Surface plasmon resonance (SPR) sensors: approaching their limits?," *Optics express,* vol. 17, no. 19, pp. 16505-16517, 2009.

[15] R. Slavík and J. Homola, "Ultrahigh resolution long range surface plasmon-based sensor," *Sensors and Actuators B: Chemical,* vol. 123, no. 1, pp. 10-12, 2007.

[16] B. Sepúlveda, A. Calle, L. M. Lechuga, and G. Armelles, "Highly sensitive detection of biomolecules with the magneto-optic surface-plasmon-resonance sensor," *Optics letters,* vol. 31, no. 8, pp. 1085-1087, 2006.

[17] A. D'Amico and C. Di Natale, "A contribution on some basic definitions of sensors properties," *IEEE Sensors Journal,* vol. 1, no. 3, pp. 183-190, 2001.

[18] C. Rizal, S. Pisana, and I. Hrvoic, "Improved magneto-optic surface plasmon resonance biosensors," *Photonics (Special Issue of Biomedical Photonics Advances),* vol. 5, no. 3, p. 116, 2018.

[19] V. N. Konopsky *et al.*, "Registration of long-range surface plasmon resonance by angle-scanning feedback and its implementation for optical hydrogen sensing," *New Journal of Physics,* vol. 11, no. 6, p. 063049, 2009.

[20] C. Rizal, S. Pisana, I. Hrvoic, and E. Fullerton, "Microstructure and magneto-optical surface plasmon resonance of Co/Au multilayers," *Journal of Physics Communications,* vol. 2, p. 055010, 2018.

[21] C. Rizal and E. Fullerton, "Perpendicular magnetic anisotropy and microstructure properties of nanoscale Co/Au multilayers," *Journal of Physics D: Applied Physics,* vol. 50, no. 35, p. 355002, 2017.

[22] C. Rizal, B. Moa, J. Wingert, and O. G. Shpyrko, "Magnetic anisotropy and magnetoresistance properties of Co/Au multilayers," *IEEE Transactions on Magnetics,* vol. 51, no. 2, pp. 1-6, 2015.

[23] https://refractiveindex.info/ [Online].

[24] E. E. Fullerton, I. K. Schuller, H. Vanderstraeten, and Y. Bruynseraede, "Structural refinement of superlattices from x-ray diffraction," *Physical Review B,* vol. 45, no. 16, p. 9292, 1992.

[25] B. Heinrich and J. A. C. Bland, *Ultrathin magnetic structures II: Measurement techniques and novel magnetic properties*. Springer Science & Business Media, 2006.

[26] D. O. Ignatyeva, G. A. Knyazev, P. O. Kapralov, G. Dietler, S. K. Sekatskii, and V. I. Belotelov, "Magneto-optical plasmonic heterostructure with ultranarrow resonance for sensing applications," *Scientific reports,* vol. 6, p. 28077, 2016.

[27] M. Björck and G. Andersson, "GenX: an extensible X-ray reflectivity refinement program utilizing differential evolution," *Journal of Applied Crystallography,* vol. 40, no. 6, pp. 1174-1178, 2007.

[28] http://www.schott.com [Online].

[29] P. Johnson and R. Christy, "Optical constants of transition metals: Ti, v, cr, mn, fe, co, ni, and pd," *Physical Review B,* vol. 9, no. 12, p. 5056, 1974.

[30] P. E. Ciddor, "Refractive index of air: new equations for the visible and near infrared," *Applied optics,* vol. 35, no. 9, pp. 1566-1573, 1996.

[31] G. M. Hale and M. R. Querry, "Optical constants of water in the 200-nm to 200-μm wavelength region," *Applied optics,* vol. 12, no. 3, pp. 555-563, 1973.

[32] J. Rheims, J. Köser, and T. Wriedt, "Refractive-index measurements in the near-IR using an Abbe refractometer," *Measurement Science and Technology*, vol. 8, no. 6, p. 601, 1997.

[33] K. Moutzouris, M. Papamichael, S. C. Betsis, I. Stavrakas, G. Hloupis, and D. Triantis, "Refractive, dispersive and thermo-optic properties of twelve organic solvents in the visible and near-infrared," *Applied Physics B*, vol. 116, no. 3, pp. 617-622, 2014.

[34] N. Sultanova, S. Kasarova, and I. Nikolov, "Dispersion proper ties of optical polymers," *Acta Physica Polonica-Series A General Physics*, vol. 116, no. 4, p. 585, 2009.